HHS Public Access

Author manuscript

J Am Chem Soc. Author manuscript; available in PMC 2020 March 13.

Published in final edited form as:

J Am Chem Soc. 2019 March 13; 141(10): 4282–4290. doi:10.1021/jacs.8b10795.

Engineering of Bioinspired, Size-Controllable, Self-Degradable Cancer-Targeting DNA Nanoflowers via the Incorporation of an Artificial Sandwich Base

Lili Zhang[†], **Razack Abdullah**[†,‡], **Xiaoxiao Hu**[†], **Huarong Bai**[†], **Huanhuan Fan**[†], **Lei He**[†], **Hao Liang**[†], **Jianmei Zou**[†], **Yanlan Liu**[†], **Yang Sun**[‡], **Xiaobing Zhang**[*,†], and **Weihong Tan**[*,†,‡,§]

[†]Molecular Science and Biomedicine Laboratory, State Key Laboratory of Chemo/Bio-Sensing and Chemometrics, College of Chemistry and Chemical Engineering, College of Life Sciences, and Aptamer Engineering Center of Hunan Province, Hunan University, Changsha, Hunan 410082, China

[‡]Institute of Molecular Medicine (IMM), Renji Hospital, Shanghai Jiao Tong University School of Medicine, and College of Chemistry and Chemical Engineering, Shanghai Jiao Tong University, Shanghai, China

[§]Department of Chemistry and Department of Physiology and Functional Genomics, Center for Research at the Bio/Nano Interface, Health Cancer Center, UF Genetics Institute and McKnight Brain Institute, University of Florida, Gainesville, Florida 32611-7200, United States

Abstract

In this article, we used an artificial DNA base to manipulate the formation of DNA nanoflowers (NFs) to easily control their sizes and functionalities. Nanoflowers have been reported as the noncanonical self-assembly of multifunctional DNA nanostructures, assembled from long DNA building blocks generated by rolling circle replication (RCR). They could be incorporated with myriad functional moieties. However, the efficacy of these DNA NFs as potential nanocarriers delivering cargo in biomedicine is limited by the bioavailability and therapeutic efficacy of their cargo. Here we report the incorporation of metal-containing artificial analogues into DNA strands to control the size and the functions of NFs. We have engineered bioinspired, size-controllable, self-degradable cancer-targeting DNA nanoflowers (Sgc8-NFs-Fc) via the incorporation of an artificial sandwich base. More specifically, the introduction of a ferrocene base not only resulted in the size controllability of Sgc8-NFs-Fc from 1000 to 50 nm but also endowed Sgc8-NFs-Fc with self- degradability in the presence of H_2O_2 via Fenton's reaction. In vitro experiments confirmed that Sgc8-NFs-Fc/Dox could be selectively taken up by protein tyrosine kinase 7 (PTK7)-positive cancer cells and subsequently cleaved via Fenton's reaction, resulting in rapid release kinetics, nuclear accumulation, and enhanced cytotoxicity of their cargo. In vivo experiments further

[*]**Corresponding Authors:** tan@chem.ufl.edu., xbzhang@hnu.edu.cn.

Author Contributions

L.Z., R.A., and X.H. contributed equally to this work.

Supporting Information

The Supporting Information is available free of charge on the ACS Publications website at DOI: 10.1021/jacs.8b10795.

Additional figures and tables as noted in text (PDF)

The authors declare no competing financial interest.

confirmed that Sgc8-NFs-Fc has good tumor-targeting ability and could significantly improve the therapeutic efficacy of doxorubicin in a xenograft tumor model. On the basis of their tunable size and on-demand drug release kinetics upon H_2O_2 stimulation, the Sgc8-NFs-Fc nanocarriers possess promising potential in drug delivery.

Graphical Abstract

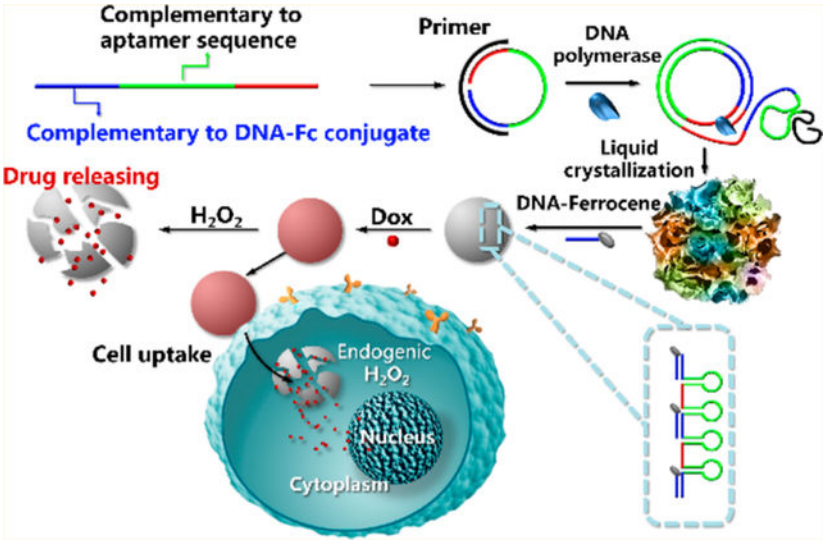

It is known that DNA and RNA are the building blocks of life, containing all of the information that cells need to synthesize proteins and replicate. In recent years, various artificial analogues have been created to add new bases for life, such as therapeutic nucleosides,[1–4] unnatural base pairs of alternative hydrogen bonding,[5,6] hydrophobic unnatural base pairs[7,8] and metal-base pairs.[9] Compared to their natural congeners, artificial bases differ in the nucleobase,[10] the sugar,[11] or the phosphate moiety.[12] Because of their resistance to nucleases, enhanced thermostability, and maneuverability, artificial bases hold great potential in disease treatment, aptamers selection, modern sequencing methods, and biometric technology.[13–17]

Our group has previously reported “the noncanonical self-assembly of multifunctional DNA nanostructures, termed as nanoflowers (NFs), assembled from long DNA building blocks generated by rolling circle replication (RCR).”[18] Although NFs have attracted significant attention in drug delivery as a result of their high drug-loading capacity, the complexity of RCR makes it hard to control their size. DNA nanoflowers are exceptionally stable in biophysiological fluids owing to the sparsity of nick sites in the elongated DNA products and the coprecipitation of DNA products and magnesium pyrophos- phate during the synthesis process. However, these properties also decrease the bioavailability and efficacy of their cargo.[18–20] Therefore, to improve the therapeutic efficacy, it is necessary to develop DNA NF-based drug delivery systems with the capability of on-demand drug release in a stimuli-responsive manner in cancer cells instead of a passive release.

Ferrocene (Fc), a metallocene, has remarkable redox properties that have been widely utilized in chemical sensors as well as biosensors. Therefore, it is not surprising that the incorporation of ferrocene moieties into DNA has become a highly attractive field of study, given the wide range of potential applications,[21] including the development of electrochemical sensors[22] and DNA nanomaterials.[23] Over the last two decades, scientists have succeeded in conjugating ferrocene with DNA through its backbone (i.e., sugar and nucleobase) in order to monitor signal changes with the aim of detecting targets.[24–28] Fc, as a key functional component, is expected to hold promise in constructing various novel DNA nanomolecules, as biomaterials, or by endowing other materials with new functions and unique applications. Most studies have reported on the linkage of the Fc group to DNA by a flexible alkyl chain or C−C connection, making it difficult to precisely identify the FC group's properties. To date, however, no studies have reported on the replacement of ferrocene on nucleobases for the purpose of studying FC properties with DNA nanoflowers. Of particular importance in the present study is the report that Fc can react with H_2O_2 to produce hydroxyl radicals through Fenton chemistry, causing breaks in DNA strands.[30,31] Adopting this idea, we herein report the engineering of bioinspired, size-controllable, and self-degradable cancer-targeting DNA nanoflowers (Sgc8-NFs- Fc) via the incorporation of an artificial sandwich base or, more specifically, the incorporation of Fc base into DNA, or Fc-DNA, with DNA NFs. On the basis of the breaks in DNA strands caused by the Fc base, Sgc8-NFs-Fc shows a Fenton's reaction-induced self-degradation capacity which efficiently improves the release kinetics, as well as the therapeutic efficacy, of anticancer drugs in cancer cells (Scheme 1). Moreover, the introduction of Fc base into DNA promotes the size controllability of Sgc8-NFs-Fc via hydrophobic interactions.

■ RESULTS AND DISCUSSION

Synthesis and Characterization of NFs-Fc.

The synthesis of Sgc8-NFs-Fc, as illustrated in Schemes 1 and 2, includes three steps: the synthesis of Fc-DNA, the preparation of DNA nanoflowers, and the incorporation/hybridization of H_2O_2-responsive Fc DNA with DNA nanoflowers. Fc-DNA was first prepared via the incorporation of Fc base into DNA. Fc base synthesis is described in the Experimental Section. Briefly, commercially available (*S*)-3-amino-1,2-propanediol was coupled with compound **1**, and the corresponding phosphoramidite (**4**) was prepared for DNA solid-phase synthesis by standard methods (Scheme 2, Figures S1 and S2). DNA nanoflowers were then prepared according to our previous reports.[18,32,33] In general, a closed circular DNA (Table S1) containing the complementary sequence of aptamer Sgc8 was utilized as the DNA template to produce an Sgc8-tandem repeat DNA sequence. The resulting long DNA sequences could spontaneously form petal-like DNA structures with a size in the micrometer range (Figure 1a) via a process of crystallization, nucleation, and growth. Subsequently, Fc-DNA (Table S1) was incorporated by hybridization with DNA sequences into the DNA nanoflowers.

The dimensional regulation of DNA nanoflowers typically involves molecular multiplication based on enzymatic amplification reaction conditions or poly(ether imide) (PEI). However, the applications of NFs are limited by their large microstructure sizes, nondegradation, and

biocompatibility. Hydrophobic interactions between hydrophobic moieties can also tightly condense nucleic acids. For example, cholesterol was used to condense RNA microparticles.[34] Therefore, it was speculated that DNA with incorporated hydrophobic Fc could be used to control the size of the DNA flowers. To investigate the effect of Fc on the size of DNA flowers, DNA flowers were analyzed via scanning electron microscopy (SEM) after incubation with Fc-DNA at different concentrations (Table S2). As shown in Figure 1a–d, the size of the DNA flowers decreased gradually with increasing Fc-DNA concentration, and DNA nanostructures with different diameters (200, 100, and 50 nm) could be easily obtained. The control of Fc-DNA over the size of DNA NFs was also confirmed by dynamic light scattering (DLS, Figure 1e). Transmission electron microscopy (TEM) also revealed that the morphology of Sgc8-NFs became gradually condensed and changed from petal-like structures with hierarchical pores to densely packed ball-like structures when the concentration of Fc-DNA increased (Figure 1f–i). These results clearly demonstrate that Fc base can be utilized to accurately control the size of DNA NFs. In general, nanoparticles with a size of less than 10 nm tend to be rapidly cleared from the body through the kidneys, whereas large nanoparticles are easily internalized by the reticuloendothelial system (RES) and accumulate in the liver or spleen. It has been suggested that nanoparticles with an average size of 50–100 nm exhibit a prolonged circulation time in the blood and subsequently improved accumulation in tumors through the EPR effect. Therefore, our Sgc8-NFs-Fc holds great promise for enhanced tumor accumulation and therapeutic efficacy, given their optimal size distribution and aptamer-mediated targeting delivery.[35,36] Because 100 nm nanoparticles could accumulate and penetrate effectively in tumor xenografts by the enhanced permeation and retention effect,[37] Sgc8-NFs-Fc with a 100 nm diameter was chosen as the drug delivery nanocarrier in this study.

The packed DNA NFs (Sgc8-NFs-Fc) still presented high resistance to nuclease cleavage like Sgc8-NFs and could be stable in 5 U/mL DNase I for 24 h (Figure S4). STEM-based EDS mapping analysis revealed that phosphorus and magnesium were uniformly distributed throughout Sgc8-NFs-Fc, indicating a mixture of phosphorus (DNA, P2O72-produced in RCR, ATP and dNTP remain) and Mg^{2+} (Figure S5). The contents of $P_2O_7^{2-}$ produced in RCR and ATP and dNTP remains were not further analyzed because of the lack of appropriate methods. However, the mass ratio of DNA/Mg^{2+}/Fc in Sgc8-NFs-Fc was 115:4.7:2.3, as determined with a Shimadzu BioSpec-nano microvolume spectrophotometer, STEM-mapping, and ICP-OES.

Self-Degradation and Drug Release from NFs-Fc.

Figure S6 demonstrates that Sgc8-NFs-Fc (23 μg) could rapidly load 0.131 micromole of Dox. The Fc could react with H_2O_2 to produce hydroxyl radicals, which could then cleave DNA. Cancer cells inside solid tumors are known to constitutively produce a high intracellular concentration of H_2O_2 (50–100 μM), which in turn enhances the neoplastic behavior by augmenting both the genetic instability of a tumor and its capacity to injure and penetrate host tissues.[38] To confirm whether Sgc8-NFs-Fc can be degraded and promote its cargo release in the presence of H_2O_2 via hydroxyl radicals produced from the Fenton reaction, we first studied the correlation between the Fenton reaction and Fc content. The reaction between Fc in Sgc8-NFs-Fc and H_2O_2 was analyzed by recording electron

paramagnetic resonance (EPR) spectra of 5-diethoxyphosphoryl-5-methyl-1-pyrroline N-oxide (DEPMPO) and its paramagnetic adduct DEPMPO-OH arising from the reaction of DEPMPO with•OH produced via the Fenton reaction. As shown in Figure S7, EPR signals were gradually enhanced by the increased concentration of Sgc8-NFs-Fc. Then the morphology of Sgc8-NFs-Fc was studied by SEM and TEM in the presence of different concentrations of H_2O_2, which was typically found in cancer cells. As shown in Figure 1a and Figure S8, no apparent change in the morphology of Sgc8-NFs was observed, either with or without H_2O_2 treatment. However, Sgc8-NFs-Fc lost its condensed ball-like morphology and was cut into pieces after treatment with H_2O_2 (Figure 1c,j and Figure S9). The damage to the Sgc8-NFs-Fc structure caused by H_2O_2 was also confirmed by the smeared band that appeared when analyzed by agarose gel electrophoresis (Figure S10). These results clearly demonstrate that Sgc8-NFs-Fc can achieve self- degradation in the presence of H_2O_2 via hydroxyl radicals produced from the Fenton reaction.

To study whether the self-degradation of Sgc8-NFs-Fc could facilitate drug release, the release of Dox from Sgc8-NFs-Fc in the presence of different concentrations of H_2O_2 was systematically investigated. As shown in Figure S11, compared to Sgc8-NFs, Sgc8-NFs-Fc with dense structures exhibited less Dox leakage in the absence of H_2O_2 but more efficient Dox release in the presence of H_2O_2, resulting in an increase in the Dox fluorescence signal in the supernatant. The cargo release of Sgc8-NFs-Fc/Dox in plasma in the presence vs absence of H_2O_2 was also investigated. As shown in Figure S12, only 18.4% of Dox was released from Sgc8-NFs-Fc/Dox after 24 h of incubation, in sharp contrast to the H_2O_2- or ultrasound-treated groups which respectively showed 59% and almost complete release of Dox from Sgc8-NFs-Fc/Dox. The results demonstrated that Sgc8-NFs-Fc/Dox had good physiological stability, and its cargo release was H_2O_2-dependent. Therefore, taken together, it can be expected that Sgc8-NFs-Fc/Dox could be stable in the circulation system and effectively release its cargo in cancer cells based on a high H_2O_2 concentration.

Selective Recognition and Internalization of Sgc8- NFs-Fc/Dox.

To demonstrate whether aptamer sgc8 in condensed Sgc8-NFs-Fc could retain its ability to recognize target protein tyrosine kinase 7 (PTK7), Ctr-NFs-Fc was prepared using a control DNA template in which a nonaptamer control DNA was substituted for the aptamer-encoding sequences in the Ctr-template. The binding abilities of Sgc8- NFs-Fc/Dox and Ctr-NFs-Fc/Dox to PTK7-positive (PTK7+) MCF-7 cancer cells, which overexpress PTK7, and PRK7- negative (PTK7-) Ramos cells, which lack PTK7, were studied. PTK7+ MCF-7 presented a 13-fold-higher fluorescence signal over that of PTK7-negative Ramos cells after incubation with Sgc8-NFs-Fc/Dox by flow cytometric analysis. However, after incubation with Ctr-NFs-Fc/Dox, MCF-7 cells and Ramos cells presented similar fluorescence signal (Figure 2a,b and Figure S13). The targeting ability of Sgc8-NFs-Fc/Dox was further validated by PTK7+ HCT-116 cells. CLSM analysis also proved that Sgc8-NFs-Fc/Dox could more efficiently recognize and enter MCF-7 cells (Figure 2c,d). These results clearly demonstrate that the incorporation of Sgc8 in Sgc8- NFs-Fc does not compromise its recognition ability and that aptamer Sgc8 can mediate the recognition and accumulation of nanocarriers in target cancer cells.

Intracellular Drug Release and Location in Cancer Cells.

To confirm that internalized Sgc8-NFs-Fc could increase intracellular ROS via the Fenton reaction, the intracellular active oxygen level was studied with an oxidative stress sensing probe, 2′,7′-dichlorofluorescin diacetate (DCFH-DA), after MCF-7 cells were incubated with Sgc8- NFs-Fc and Sgc8-NFs_{3h}, which were prepared by rolling circle replication for 3 h. As shown in Figure S14, MCF-7 cells treated with Sgc8-NFs-Fc presented brighter fluorescence signals than did MCF-7 cells and MCF-7 cells treated with Sgc8-NFs_{3h}. The results suggested that internalized Sgc8-NFs-Fc could catalyze the conversion of intracellular H_2O_2 to hydroxyl radicals, which were expected to degrade the nanocarrier and promote cargo release. Therefore, the cargo release of Sgc8-NFs-Fc/Dox in MCF-7 cells was further investigated and compared to that of Sgc8-NFs_{3h}/Dox, which was prepared according to a previous report (Figure S15).[33] Sgc8-NFs_{3h} stands for the smallest nanoparticles without Fc- DNA bases obtained after RCR for 3 h. Dox delivered by Sgc8-NFs-Fc could rapidly accumulate in the cellular nucleus within 30 min of incubation (Figure S16). However, Dox delivered by Sgc8-NFs_{3h} had no obvious accumulation in the nucleus, even after 1 h of incubation. In addition, the rapid nuclear accumulation of Dox delivered by Sgc8-NFs-Fc was not observed in the noncancerous HEK293 cell line (Figure S17), a result that could be ascribed to the low concentration of intracellular H_2O_2[39] These results support our hypothesis that an Fc-based nanocarrier can interact with H_2O_2 in cancer cells, produce hydroxyl radicals, and consequently degrade the DNA nanocarrier for an efficient release of payload.

To further prove this hypothesis, the concentration of intracellular H_2O_2 was mediated by pretreating MCF-7 cells with H_2O_2 stimulant phorbol-12-myristate-13-acetate (PMA)[40] or H_2O_2 scavenger *N*-acetyl-L-cysteine (NAC).[41] As shown in Figure 3, MCF-7 cells pretreated with PMA obviously had a stronger fluorescence signal in the nucleus and a weaker fluorescence signal in the cytoplasm when compared to those of native MCF-7 cells after incubation with Sgc8-NFs- Fc/Dox. However, MCF-7 cells treated with NAC obviously had an increased cytoplasmic fluorescence signal and a decreased nuclear fluorescence signal compared to those of MCF-7 cells. In addition, the distribution of Dox in the cytoplasm and nucleus caused no obvious changes in MCF-7 cells treated with PMA or NAC compared to MCF-7 cells after incubation with Sgc8-NFs_{3h}/Dox. These results clearly indicate that H_2O_2 stimulant PMA enhances the release of Dox from the nanocarrier, whereas H_2O_2 scavenger NAC inhibits its release. Meanwhile, MCF-7 cells were pretreated with H_2O_2, followed by incubation with Sgc8-NFs-Fc/Dox or Sgc8-NFs_{3h}/Dox. Among these, MCF-7 cells incubated with Sgc8-NFs-Fc/ Dox, instead of MCF-7 cells incubated with Sgc8-NFs_{3h}/Dox, had a decreased cytoplasmic distribution and an increased nuclear distribution of Dox (Figure S18). These results strongly prove that Fenton's reaction between Fc and intracellular H_2O_2 facilitates the release of Dox from Sgc8-NFs-Fc/Dox and the accumulation of Dox in the nucleus.

Therapeutic Efficacy in Vitro.

The cytotoxicity of Sgc8-NFs-Fc/Dox in MCF-7 cells and Ramos cells was evaluated and compared with that of Sgc8-NFs-Fc, free Dox, Sgc8-NFs_{3h}/Dox, and Ctr-NFs-Fc/Dox. Sgc8-NFs-cholesterol (Sgc8-NFs-Chol), which was prepared by the replacement of Fc-DNA

with cholesterol-labeled DNA,[16] and Sgc8-NFs-Chol/ Dox were also used as controls (Figure S19). As shown in Figure 4a, Sgc8-NFs-Fc/Dox exhibited stronger cytotoxicity to PTK7+ MCF-7 cells than did nanocarrier Sgc8-NFs-Fc and four other drug formulations (free Dox, Sgc8-NFs_{3h}/Dox, Sgc8-NFs-Chol/Dox, and Ctr-NFs-Fc/Dox). These results were identical to those confirmed for PTK7+ HCT-116 cells (Figure S20). However, Sgc8-NFs-Fc/Dox exhibited cytotoxicity on PTK7-Ramos cells similar to that of Ctr-NFs-Fc/Dox, but with less cytotoxicity than for free Dox (Figure 4b). The cytotoxic differences in MCF-7 cells and Ramos cells between Sgc8-NFs-Fc/Dox and free Dox might arise from their different cellular uptake in cells (Figure S21): Sgc8-NFs-Fc/ Dox increased the accumulation of Dox in MCF-7 cells but decreased the accumulation of Dox in Ramos cells. This line of evidence suggests that Sgc8-NFs-Fc/Dox not only enhances the cytotoxicity of Dox on target cancer cells but also decreases the cytotoxicity of Dox on nontarget cancer cells. The enhanced performance of nanodrugs could be ascribed to the specific targeting of cancer cells and efficient drug release.

Antitumor Activity of Sgc8-NFs-Fc/Dox Nanoparticles in Vivo.

As one of the most important factors that determined the biodistribution and target activity of Sgc8-NFs-Fc in in vivo experiences, the plasma stability of Sgc8-NFs-Fc was first studied. As shown in Figure S12 and Figure S22, Sgc8-NFs-Fc/ Dox remained relatively stable in plasma within 24 h, demonstrating its potential for in vivo studies. To test the in vivo tumor-targeting ability of nanocarrier Sgc8-NFs-Fc, mice bearing PTK7+ HCT-116 tumors were imaged after intravenous injections of Sgc8-NFs-Fc/TMPYP4, Ctr-NFs-Fc/TMPYP4, or free TMPYP4, respectively. As shown in Figure S23, TMPYP4 was used as a low toxicity dye because it could be excited and detected by the IVIS Lumina II Imaging System. Figure S24 shows that the active targeting of PTK7 by Sgc8-NFs-Fc/TMPYP4 could clearly cause fluorescence signals in tumors 5 min and even 3 h postinjection. However, only marginally fluorescent signals in tumors were observed after the injection of TMPYP4 or Ctr-NFs-Fc/TMPYP4. The fluorescence imaging of the excised tumors and other main organs, including the heart, liver, kidneys, spleen, lungs, and intestines, also proved that Sgc8-NFs-Fc/TMPYP4 caused a greater payload accumulation in tumors but decreased accumulation in the liver, kidneys, and spleen when compared to Ctr-NFs-Fc (Figure S25). These results demonstrate that Sgc8-NFs-Fc has specific cancer-targeting ability. The nanocarriers could be quickly removed from the body and hence cause only negligible side effects (Figure S26).

We further evaluated the antitumor activity of Sgc8-NFs-Fc/ Dox in an HCT-116 s.c. mouse xenograft tumor model. When tumor nodules grew to 60–70 mm^3, the mice were divided into seven groups for comparative efficacy studies in which the following regimens were administered by intratumoral injections every other day: D-PBS only (i), free Dox (ii), Sgc8-NFs-Fc (iii), Sgc8-NFs_{3h}/Dox (iv), Sgc8-NFs-Chol/Dox (v), Ctr-NFs-Fc/Dox (vi), and Sgc8-NFs-Fc/Dox (vii). The Dox dosage was 0.5 mg/kg in groups ii and iv−vii for the first week and 1 mg/kg for the last 2 weeks. The tumor size was monitored and photographed every day after injection. As shown in Figure 4c and Figures S27 and S28, the tumor treated with only D-PBS or Sgc8-NFs-Fc sharply increased and reached ~1600 mm^3 or ~1400 mm^3 in size after a 21-day treatment, respectively. The results indicate that these nanocarriers had

only a marginal anticancer effect. When treated with five other Dox formulations (free Dox, Sgc8-NFs_{3h}/Dox, Sgc8-NFs-Chol/Dox, Ctr-NFs-Fc/Dox, and Sgc8-NFs-Fc/Dox), the tumor in each group presented slower growth than tumors treated with D-PBS and Sgc8-NFs-Fc. Among these Dox formulations, Sgc8-NFs-Fc/Dox had better antitumor efficacy than either nontargeting Dox formulations (free Dox and Ctr-NFs-Fc/Dox) or PTK7-targeting Dox formulations (Sgc8-NFs_{3h}/Dox and Sgc8-NFs-Chol/Dox) when tested on tumor volumes of ~500 mm^3 during a 21-day treatment. H&E staining of tumor slices also proved that Sgc8-NFs-Fc/Dox had excellent antitumor capability compared to that of other Dox formulations. Moreover, no significant drop in body weight and no obvious damage to major organs were observed in mice treated with Sgc8-NFs-Fc/Dox (Figure 4d and Figure S29). The in vivo results demonstrate that Sgc8-NFs-Fc has cancer-targeting ability and can improve the therapeutic efficacy of its cargo.

■CONCLUSIONS

A size-controllable and bioinspired self-degradable, cancer-targeting DNA NFs-based Sgc8-NFs-Fc nanocarrier has been developed to improve the bioavailability and therapeutic efficacy of small-molecule drugs. Sgc8-NFs-Fc was prepared by incorporating Fc-DNA with DNA NFs via hybridization. The size of Sgc8-NFs-Fc could be easily controlled by changing the amount of hydrophobic Fc-base-containing Fc DNA. As-prepared Sgc8-NFs-Fc had a high drug-loading capability for Dox and could specifically recognize and accumulate in PTK7+ cancer cells. Furthermore, Sgc8-NFs-Fc could self-degrade via Fenton's reaction in cancer cells. The self-degradation of the nanocarrier could promote drug release, resulting in more nuclear accumulation and cytotoxicity of Dox. In vivo experiments also demonstrated that Sgc8-NFs-Fc could efficiently deliver its cargo to tumors and reduce the nonspecific distribution of cargo in normal organs while improving the therapeutic efficacy of Dox. On the basis of the high concentration of H_2O_2, a hallmark of cancer cells, our study is believed to provide a facile strategy for the rational design of smarter nanocarriers to overcome the challenges of low bioavailability and therapeutic efficacy in cancer therapy.

■ EXPERIMENTAL SECTION

Materials and Reagents.

All oligonucleotide sequences, except for ferrocene DNA, were purchased from Sangong Biotech Inc. (Shanghai, China) and purified by HPLC. A Cell Titer 96 AQueous One Solution Cell Proliferation Assay (MTS) was purchased from Promega Corporation. Hoechst 33342, Phorbol-12-myristate-13-acetate (PMA), and N-acetylcysteine (NAC) were purchased from Beyotime Institute of Biotechnology (Shanghai, China). Doxorubicin (Dox) was purchased from Sangon (Shanghai, China). 2′,7′-Dichlorofluorescin diacetate (DCFH-DA) was purchased from Sigma-Aldrich (Taufkirchen, Germany). All other reagents were analytical grade and used without further purification. The ultrapure water used was from a Milli-Q Integral System.

All reagents were used as received from commercial sources or prepared as described in references. Anhydrous solvents pyridine, CH_3CN, CH_2Cl_2, and DMF were distilled under a

nitrogen atmosphere and stored with 4 Å molecular sieves.^{1}H spectra were recorded on a Bruker AM300 spectrometer.^{13}C NMR spectra were recorded on a Bruker AM400 spectrometer. Chemical shifts (δ) are reported in ppm, and coupling constants (J) are in Hertz (Hz). The following abbreviations were used to explain the multiplicities: s = singlet, d = doublet, t = triplet, q = quartet, m = multiplet, and br = broad.

Synthesis of Ferrocene Base. Synthesis of Compound 2.—Ferrocene carboxylic acid **1** (1 g, 4.34 mmol) was coupled with *S*-aminopropanediol (0.39 g, 4.34 mmol) in the presence of diisopropylethylamine (0.84 g, 6.51 mmol) and 2-(1*H*-benzotriazol-1-yl)-1,1,3,3-tetramethyluronium hexafluorophosphate (HBTU, 1.64 g, 4.34 mmol) in dry DMF. After the reaction mixture was stirred at room temperature for 3 h, the solvent was removed, and the crude residue was purified with silica gel column chromatography (dichloromethane/methanol = 95:5, R_f = 0.3) to offer the desired product, **2**, in 95% yield.

Synthesis of Compound 3.—Compound **2** (1 g, 3.30 mmol) was dissolved in dry pyridine in an ice bath under nitrogen. Then 4,4′- dimethoxytrityl chloride (1.34 g, 3.96 mmol) in CH_2Cl_2 was added to the above mixture. After 30 min of vigorous stirring, the reaction mixture became transparent. Then the ice bath was removed, and the reaction mixture was further stirred at room temperature. After 12 h, the solvent was removed by evaporation, and the obtained solid was subjected to silica gel column chromatography (AcOEt/hexane/Et_3N = 35:65:1, R_f = 0.5) to offer the desired product, 3, in 60% yield.

Synthesis of Compound 4.—To a solution of compound **3** (1 g, 1.65 mmol) in anhydrous DCM (15 mL) was added diisopropyl-ethylamine (0.43 g, 3.30 mmol), followed by chlorophosphoramidite (0.47 g, 1.98 mmol) at 0 °C. The mixture was allowed to warm to RT and stirred for 1 h. Then the reaction mixture was diluted with 5 mL of DCM and washed with saturated $NaHCO_3$ solution and saturated saline solution. The organic phase was dried over Na_2SO_4 and then concentrated in vacuo. The residue was subjected to silica gel column chromatography (AcOEt/hexane/Et_3N = 20:80:1, R_f = 0.5) to offer the desired product, **4**, as a yellow foam in 75% yield (mixture of diastereoisomers).

Ferrocene DNA Synthesis.—Using the corresponding controlled pore glass (CPG), the ferrocene DNA strand used in this work was synthesized on the Polygen 12-column DNA/RNA solid synthesizer on a 1.0 μM scale. As-synthesized ferrocene phosphoramidite monomer was dissolved in anhydrous dichloromethane to 0.1 M concentration and coupled on the synthesizer after 300 s of coupling time. After synthesis, the obtained oligonucleotides were cleaved and deprotected from the CPG, followed by precipitation in cold ethanol solution at −20 °C overnight. After centrifugation to remove the supernatant solution, the DNA products were dissolved with 0.1 M TEAA and purified by reverse-phase HPLC using a BioBasic4 column. Finally, the 4,4′-dimethytrityl group was removed from DNA by adding an 80% acetic acid aqueous solution, and the DNA was again precipitated in cold ethanol. After drying in vacuum and undergoing desalting, the synthesized oligonucleotides were quantified by measuring their absorbance at 260 nm.

Cell Culture and Buffers.—The MCF-7 and HEK293 cell lines were cultured in DMEM medium (Gibco). The HCT-116 and Ramos cell lines were cultured in RPMI 1640 medium

(Gibco). All types of media were supplemented with 10% FBS (Gibco) and 1% antibiotic (Gibco). Cells were cultured at 37 °C in a humid atmosphere with 5% CO_2. Dulbecco's phosphate-buffered saline without Ca^{2+} and Mg^{2+} (D-PBS, Gibco) was used to wash cells. The number of cells was determined by a hemocytometer prior to each experiment.

Washing buffer was prepared with D-PBS supplemented with 4.5 g/L glucose and 5 mM $MgCl_2$. Binding buffer was prepared with washing buffer supplemented with 0.1 mg/mL yeast tRNA (Sigma-Aldrich) and 1 mg/mL BSA (Fisher Scientific). Tris-HCl used in this study was 50 mM Tris-HCl containing 10 mM $MgCl_2$ (pH 7.9).

General Characterization.—Dynamic light scattering (DLS) and the zeta potential were measured on a Malvern Zetasizer Nano ZS90 (Malvern Instruments, Ltd., Worcestershire, U.K.). Transmission electron microscopy (TEM) was carried out on an H-7000 NAR transmission electron microscope (Hitachi) with a working voltage of 100 kV. Scanning electron microscope (SEM) analysis was performed on an S-4800 scanning electron microscope (Hitachi, Japan). Fluorescence was observed using a Fluoromax-4 spectrofluorometer (Horiba, JobinYvon, Edison, NJ).

Self-Assembly of DNA Nanoflowers Using RCR.—DNA nanoflowers were prepared according to our previous reports.[15] A phosphorylated linear template (0.6 μM) and a primer (1.2 μM) were mixed in DNA ligation buffer (50 mM Tris-HCl, 1 mM $MgCl_2$, 0.1 mM ATP, and 1 mM dithiothreitol) and annealed at 95 °C for 5 min, followed by gradual cooling to room temperature over 1 h. The annealed product was incubated with *E. coli* DNA ligase (10 U/μL; Takara Bio, Dalian, China) at 16 °C for 4 h. For RCR, the circularized template (0.3 μM, unless otherwise denoted) was incubated with Φ29 DNA polymerase (2 U/μL), dNTP (2 mM), and BSA (1×) in buffer solution (50 mM Tris-HCl, 10 mM $(NH_4)_2SO_4$, 10 mM $MgCl_2$, and 4 mM dithiothreitol) (New England Biolabs, Ipswich, MA) at 30 °C. Sgc8-NFs_{3h} and Sgc8-NFs were formed after RCR reaction for 3 and 24 h, respectively. The RCR reaction was terminated by holding at 75 °C for 10 min. The DNA nanoflowers were then washed with doubly distilled H_2O, precipitated by centrifugation, and stored at 4 °C for future use. The as-prepared product was analyzed by agarose gel electrophoresis. The DNA concentration was quantified using the Shimadzu BioSpec-nano microvolume spectrophotometer (Kyoto, Japan).

Preparation of Sgc8-NFs-Ferrocene (Sgc8-NFs-Fc).—Sgc8-NFs-Fc was prepared by adding Fc-labeled DNA to 5 μL of Sgc8-NFs (5.5 μg) (Table S1). The mixture was held to 95 °C for 5 min to denature Sgc8-NFs and then slowly cooled to 4 °C for 2 h, yielding Sgc8-NFs-Fc. The size of the Sgc8-NFs-Fc could be accurately controlled according to the concentration of Fc-DNA. Accordingly, 100 nm Sgc8-NFs-Fc prepared by adding 5 μL of Fc-DNA to 5 μL of Sgc8-NFs was chosen for subsequent experiments. The as-prepared product was analyzed by agarose gel electrophoresis.

Preparation of Sgc8-NFs-cholesterol (Sgc8-NFs-Chol).—Sgc8-NFs-Chol was prepared by adding 5 μL of Tris-HCl buffer and 10 μL of Chol-labeled DNA dissolved in Tris-HCl buffer (370 μM) to 5 μL of Sgc8-NFs (5.5 μg). The mixture was held at 95 °C for 5 min to denature Sgc8-NFs and then slowly cooled to 4 °C for 2 h, yielding Sgc8-NFs-Chol.

Encapsulation of Dox in Sgc8-NFs-Fc.—To encapsulate Dox, 20 μL of Sgc8-NFs-Fc (23 μg) was mixed with Dox (1 mM) in D-PBS to a final volume of 200 μL. After incubation at room temperature for 24 h, Sgc8-NFs-Fc were pelleted at 10 000 rpm for 15 min, and free Dox in the supernatant was isolated and quantified by measuring the Dox fluorescence (Ex: 490 nm; Em: 590 nm). The amount of Dox loaded into Sgc8-NFs-Fc was calculated by subtracting the amount of Dox in the supernatant from the total amount of Dox. The precipitate (Sgc8- NFs-Fc/Dox) was then dispersed in D-PBS or Tris-HCl (200 μL). Sgc8-NFs/Dox was prepared with the same procedure.

Electron Paramagnetic Resonance (EPR) Measurements.—5-Diethoxyphosphoryl-5-methyl-1-pyrroline N-oxide (DEPMPO) was used as a trap for $^{\bullet}OH$ radicals. The $^{\bullet}OH$ radicals were produced by Sgc8-NFs-Fc in the presence of H_2O_2 via the Fenton reaction. For EPR measurements, different concentrations of Sgc8-NFs-Fc solution were added to 15 μL of Tris-HCl solution containing EDTA (0.2 mM), DEPMPO (40 mM), and H_2O_2 (50 μM), and the EPR spectra were recorded.

Stability of Sgc8-NFs-Fc in the Presence of Different Concen- trations of H_2O_2.—To study the stability of Sgc8-NFs-Fc, Sgc8-NFs-Fc in 200 μL of Tris-HCl was mixed with different concentrations of H_2O_2 (0, 10, 30, 50, and 100 μM). After incubation for 3 h at 25 °C, the samples was characterized by TEM and SEM.

Dox Release from Sgc8-NFs-Fc/Dox in the Presence of H_2O_2.—H_2O_2-responsive Dox release from Sgc8-NFs-Fc/Dox was analyzed according to a previous report[39] with minor modification. Briefly, Sgc8-NFs-Fc/Dox in 200 μL of Tris-HCl was mixed with different concentrations of H_2O_2 (0, 1, 5, 10, 20, 30, and 40 μM). After incubation for 3 h at 25 °C, the fluorescence intensity of samples was measured with a Fluoromax-4 spectrofluorometer (Ex: 490 nm; Em: 590 nm). For the drug release kinetics study, both Sgc8-NFs-Fc/Dox and Sgc8-NFs/Dox were treated with 0 and 50 μM H_2O_2 for 3 h. During the incubation, 2 μL of aliquots were taken out at the indicated times for fluorescence measurements. Data points for each sample were fit by nonlinear regression using Origin 8 software (Northampton, MA). In the Dox release profile, the data set is normalized with the fluorescence signal of Dox successively released from Sgc8-NFs-Fc treated with 50 μM H_2O_2 as 100%. Other curves are drawn to scale.

Flow Cytometric Analysis.—A total of 2×10^5 cells (MCF-7 or Ramos cells) were washed with washing buffer via centrifugation at 1000 rpm and then incubated with Sgc8-NFs-Fc/Dox or Ctr-NFs-Fc/ Dox in 200 μL of binding buffer at 4 °C for 1 h of binding assay. After washing twice with washing buffer (4 °C), the samples were collected and then resuspended in binding buffer for flow cytometry analyses and confocal microscopy measurements. Flow cytometry was performed with a BD FACS Verse system. Data were analyzed with Flow Jo software (Tree Star, Inc., Ashland, OR).

Confocal Laser-Scanning Microscopy Imaging (CLSM).—For adhesive MCF-7 cells or HEK293 cells without pretreatment, 1×10^5 cells were seeded in confocal dishes and cultured for 24 h, followed by incubation with Sgc8-NFs-Fc/Dox and Sgc8-NFs_{3h}/Dox (10 μM equivalent Dox) for a prescribed time. For MCF-7 cells treated with PMA, NAC, or

H_2O_2, 1 × 10 cells were seeded in confocal dishes, cultured for 24 h, and then pretreated with these chemical reagents for a specified time before incubation with Dox- loaded nanocarriers, respectively. For suspended cells, 2×10^5 Ramos cells were incubated with Dox-loaded nanocarriers for a certain time, followed by the removal of the nanocarriers and washing with D-PBS. Cells were imaged with an FV1000-X81 confocal microscope (Olympus, Japan) after washing twice with washing buffer.

CLSM Imaging of the Fenton Reaction in Cells.—MCF-7 cells (1×10^5) were seeded in confocal dishes and cultured for 24 h, followed by incubation with Sgc8-NFs-Fc and Sgc8-NFs_{3h} (5 μg) for 3 h. After washing twice with washing buffer, the cells were incubated with 5 μM DCFH-DA for 30 min. Thereafter, the cells were washed with 4 °C PBS twice and stained with Hoechst 33342 (1 μg/mL) for 10 min. After washing with 4 °C PBS twice, the cells were immediately observed via CLSM.

In Vitro Cytotoxicity Assay.—MCF-7 cells were seeded in a 96-well plate at a density of 1×10^4 cells per well. After 24 h of culture, cells were treated with Sgc8-NFs_{3h}/Dox, Sgc8-NFs-Fc/Dox, Ctr-NFs-Fc/Dox, Sgc8-NFs-Chol/Dox, free Dox, and Sgc8-NFs-Fc for 3 h, respectively. The supernatant was then removed, and fresh medium was added to the cells. After another 24 h of incubation, the medium was removed, and the cells were treated with 100 μL of medium and 20 μL of MTS for 1 to 2 h. Finally, the absorbance of the solution at 490 nm was recorded with a Synergy 2 Multi-Mode Microplate Reader (Bio-Tek, Winooski, VT). The results were repeated in triplicate, and the error bars represent the standard derivations.

Cellular Uptake Studies.—MCF-7 cells (1×10^5) or Ramos cells (2×10^5) were seeded in confocal dishes and cultured for 24 h, followed by incubation with free Dox and Sgc8-NFs-Fc/Dox (5 μM equivalent Dox) for 3 h. The cells were then washed with PBS twice and stained with Hoechst 33342 (1 μg/mL) for 10 min. After washing with PBS twice, the cells were immediately observed on CLSM.

Stability of Sgc8-NFs-Fc/Dox in the Plasma.—Mouse plasma was collected with sodium heparin and stored at −70 ± 10 °C until use. The size of Sgc8-NFs-Fc/Dox (200 μM equivalent Dox) in the plasma-containing (10%) D-PBS buffer was determined by DLS at specific times (0, 1, 2, 4, 8, 12, and 24 h). The results were analyzed using Origin 8 software. Furthermore, the stability of Sgc8-NFs-Fc/ Dox in the medium and plasma was studied by monitoring the release of Dox for 24 h. Sgc8-NFs-Fc/Dox was smashed by ultrasonic cell disruptor SCIENTZ-950E (200 W) for 1 min.

Animal Model.—The HCT-116 xenograft model[42] was established using BALB/c nude mice at 4 to 6 weeks of age. Female Balb/c mice (~20 g) were obtained from Hunan SJA Laboratory Animal Co., Ltd. and managed under protocols approved by the Hunan University Laboratory Animal Center. HCT-116 cells (10^7) in 100 μL of D-PBS were injected into the right flank of mice. Tumors were allowed to grow to 60–70 mm^3 before treatment.

In Vivo Fluorescence Imaging.—Tumor-bearing BALB/c nude mice were anesthetized with anesthetic. Once the mice were anesthetized to be motionless, 4.5 nmol of Sgc8-NFs-Fc/TMPYP4 or Ctr-NFs-Fc/ TMPYP4 was injected intravenously and percutaneously via the tail vein and percutaneous injection. At 0, 5, 30, 60, and 180 min, fluorescence images of live mice were collected with an IVIS Lumina II in vivo imaging system (Caliper Life Science, USA). After in vivo imaging, mice were sacrificed, and the major organs, including the tumor, liver, heart, lung, spleen, kidneys, and intestines, were dissected and imaged.

To investigate the retention time of nanocarriers in tumors, Sgc8- NFs-Fc/TMPYP4 was directly injected into tumors, and then the tumor retention time was characterized by imaging at indicated time intervals.

In Vivo Treatment.—When the tumor size reached ~60 mm^3, 25 μL of drug was intratumorally injected into the tumor-bearing mice. HCT-116 tumor-bearing mice were divided into seven groups of four animals per group to quantify the growth rate of tumors after the following treatments: (i) D-PBS only, (ii) free Dox, (iii) Sgc8-NFs-Fc, (iv) Sgc8-NFs_{3h}/Dox, (v) Sgc8-NFs-Chol/Dox, (vi) Ctr-NFs-Fc/ Dox, and (vii) Sgc8-NFs-Fc/Dox. The Dox dosage was 0.5 mg/kg in groups ii and iv−vi for the first week and 1 mg/kg for the last 2 weeks, as has been reported for use in this mouse strain.[43] The Sgc8-NFs-Fc dosage was kept the same as that of group vii. The tumor size and body weight were monitored every day. The size of the tumors was measured with calipers every day after treatment.

The mass and size of each mouse were monitored daily for 3 weeks after treatment and compared with those of the control mice (D-PBS- injected). The size of tumors was measured with calipers. The volume of the tumor (V) was calculated to be $V = AB^2/2$, where A and B are the longer and shorter diameters (mm) of the tumor, respectively. The relative volume of the tumors was evaluated by normalizing the measured values to their initial sizes. Statistical analysis for all in vivo experiments was carried out with one-way ANOVA (SPSS). All statistical tests were two-sided, and P values of <0.05 were considered to be significant (Figure 4c and Figure S30). The sections of kidney, liver, spleen and tumor tissues collected from the mice 3 weeks after injection were then embedded in a protective tissue-freezing medium (Tissue Tek OCT compound, Sakura Finetek, Inc., CA, USA) and frozen at −80 °C. The samples were sectioned into slides of 8 μm thickness and stained with hematoxylin and eosin (H&E) for analysis.

Supplementary Material

Refer to Web version on PubMed Central for supplementary material.

■ ACKNOWLEDGMENTS

This work was supported by the National Natural Science Foundation of China (Grants NSFC 21827811, 21325520, 21327009, J1210040, and 31701249), by US NIH GM Maximizing Investigators' Research Award R35 127130 and NSF 164521, and by the Science and Technology Project of Hunan Province (2017XK2103, 2016RS2009, 2016WK2002, and 2017DK2011).

REFERENCES

(1). Vivet-Boudou V; Didierjean J; Isel C; Marquet R Nucleoside and nucleotide inhibitors of HIV-1 replication. Cell. Mol. Life Sci 2006, 63, 163–186. [PubMed: 16389458]

(2). Schaeffer HJ; Beauchamp L; de Miranda P; Elion GB; Bauer DJ; Collins P 9-(2-hydroxyethoxymethyl) guanine activity against viruses of the herpes group. Nature 1978, 272, 583–585. [PubMed: 205792]

(3). Boyd MR; Bacon TH; Sutton D; Cole M Antiherpesvirus activity of 9-(4-hydroxy-3-hydroxy-methylbut-1-yl) guanine (BRL 39123) in cell culture. Antimicrob. Agents Chemother 1987, 31, 1238–1242. [PubMed: 3631945]

(4). Elion GB; Furman PA; Fyfe JA; de Miranda P; Beauchamp L; Schaeffer HJ The selectivity of action of an antiherpetic agent, 9-(2-hydroxyethoxymethyl) guanine. Rev. Med. Virol 1999, 9, 147–153. [PubMed: 10479776]

(5). Rappaport HP The 6-thioguanine/5-methyl-2-pyrimidinone base pair. Nucleic Acids Res. 1988, 16, 7253–7267. [PubMed: 3412886]

(6). Switzer C; Moroney SE; Benner SA Enzymatic incorporation of a new base pair into DNA and RNA. J. Am. Chem. Soc 1989, 111, 8322–8323.

(7). Hirao I; Kimoto M; Mitsui T; Fujiwara T; Kawai R; Sato A; Harada Y; Yokoyama S An unnatural hydrophobic base pair system: site-specific incorporation of nucleotide analogs into DNA and RNA. Nat. Methods 2006, 3, 729–735. [PubMed: 16929319]

(8). Leconte AM; Hwang GT; Matsuda S; Capek P; Hari Y; Romesberg FE Discovery, characterization, and optimization of an unnatural base pair for expansion of the genetic alphabet. J. Am. Chem. Soc 2008, 130, 2336–2343. [PubMed: 18217762]

(9). Meggers E; Holland PL; Tolman WB; Romesberg FE; Schultz PG Structure of a copper-mediated base pair in DNA. J. Am. Chem. Soc 2000, 122, 10714–10715.

(10). Li LJ; Degardin M; Lavergne T; Malyshev DA; Dhami K; Ordoukhanian P; Romesberg FE Natural-like Replication of an Unnatural Base Pair for the Expansion of the Genetic Alphabet and Biotechnology Applications. J. Am. Chem. Soc 2014, 136, 826–829. [PubMed: 24152106]

(11). Pinheiro VB; Taylor AI; Cozens C; Abramov M; Renders M; Zhang S; Chaput JC; Wengel J; Peak-Chew SY; McLaughlin SH; Herdewijn P; Holliger P Synthetic genetic polymers capable of heredity and evolution. Science 2012, 336, 341–344. [PubMed: 22517858]

(12). Korlach J; Bibillo A; Wegener J; Peluso P; Pham TT; Park I; Clark S; Otto GA; Turner SW Chemical Synthesis and Enzymatic Incorporation of Artificial Nucleotides. Nucleosides, Nucleotides Nucleic Acids 2008, 27, 1072–1083. [PubMed: 18711669]

(13). Sheng P; Yang Z; Kim Y; Wu Y; Tan W; Benner SA Design of a novel molecular beacon: modification of the stem with artificially genetic alphabet. Chem. Commun 2008, 41, 5128–5130.

(14). Jin C; Fu T; Wang R; Liu H; Zou J; Zhao Z; Ye M; Zhang X; Tan W Fluorinated molecular beacons as functional DNA nanomolecules for cellular imaging. Chem. Sci 2017, 8, 7082–7086. [PubMed: 29147537]

(15). Sefah K; Yang Z; Bradley KM; Hoshika S; Jiménez E; Zhang L; Zhu G; Shanker S; Yu F; Turek D In vitro selection with artificial expanded genetic information systems. Proc. Natl. Acad. Sci. U. S. A 2014, 111, 1449–1454. [PubMed: 24379378]

(16). Liu S; Clever GH; Takezawa Y; Kaneko M; Tanaka K; Guo X; Shionoya M Direct conductance measurement of individual metallo-DNA duplexes within single-molecule break junctions. Angew. Chem 2011, 123, 9048–9052.

(17). Metzker ML The Importance of Marine Genomics to Life. Nat. Rev. Genet 2010, 11, 31–46. [PubMed: 19997069]

(18). Zhu G; Hu R; Zhao Z; Chen Z; Zhang X; Tan W Noncanonical self-assembly of multifunctional DNA nanoflowers for biomedical applications. J. Am. Chem. Soc 2013, 135, 16438–16445. [PubMed: 24164620]

(19). Zhu G; Mei L; Vishwasrao HD; Jacobson O; Wang Z; Liu Y; Yung BC; Fu X; Jin A; Niu G; Wang Q; Zhang F; Shroff H; Chen X Intertwining DNA-RNA nanocapsules loaded with tumor neoantigens as synergistic nanovaccines for cancer immunotherapy. Nat. Commun 2017, 8, 1482. [PubMed: 29133898]

(20). Ni QQ; Zhang FW; Zhang YL; Zhu GZ; Wang Z; Teng ZG; Wang CY; Yung BC; Niu G; Lu GM; Zhang LJ; Chen XY In Situ shRNA Synthesis on DNA-Polylactide Nanoparticles to Treat Multidrug Resistant Breast Cancer. Adv. Mater 2018, 30, 1705737.

(21). Van Staveren DR; Metzler-Nolte N Bioorganometallic chemistry of ferrocene. Chem. Rev 2004, 104, 5931–5985. [PubMed: 15584693]

(22). Drummond TG; Hill MG; Barton JK Electrochemical DNA sensors. Nat. Biotechnol 2003, 21, 1192–1199. [PubMed: 14520405]

(23). Abi A; Lin M; Pei H; Fan C; Ferapontova EE; Zuo X Electrochemical switching with 3D DNA tetrahedral nanostructures self-assembled at gold electrodes. ACS Appl. Mater. Interfaces 2014, 6, 8928–8931. [PubMed: 24802004]

(24). Takenaka S; Uto Y; Kondo H; Ihara T; Takagi M Electrochemically active DNA probes: detection of target DNA sequences at femtomole level by high-performance liquid chromatography with electrochemical detection. Anal. Biochem 1994, 218, 436–443. [PubMed: 7521145]

(25). Sonogashira K; Tohda Y; Hagihara N A Convenient Synthesis of Acetylenes: Catalytic Substitutions of Acetylenic Hydrogen with Bromoalkenes, Iodoarenes and Bromopyridines. Tetrahedron Lett. 1975, 16, 4467–4470.

(26). Nakayama M; Ihara T; Nakano K; Maeda M DNA sensors using a ferrocene-oligonucleotide conjugate. Talanta 2002, 56, 857–866. [PubMed: 18968564]

(27). Yu CJ; Yowanto H; Wan J; Meade TJ; Chong Y; Strong MN; Donilon LH; Kayyem JF; Gozin M; Blackburn GF Uridine-Conjugated Ferrocene DNA Oligonucleotides: Unexpected Cyclization Reaction of the Uridine Base. J. Am. Chem. Soc 2000, 122, 6767–6768.

(28). Yu CJ; Wang H; Wan Y; Yowanto H; Kim JC; Donilon LH; Tao C; Strong M; Cong Y 2'-Ribose-Ferrocene Oligonucleotides for Electronic Detection of Nucleic Acids. J. Org. Chem 2001, 66, 2937–2942. [PubMed: 11325257]

(29). Clarke J; Wu HC; Jayasinghe L; Patel A; Reid S; Bayley H Continuous base identification for single-molecule nanopore DNA sequencing. Nat. Nanotechnol 2009, 4, 265–270. [PubMed: 19350039]

(30). Lopez-Lazaro M Dual role of hydrogen peroxide in cancer: possible relevance to cancer chemoprevention and therapy. Cancer Lett. 2007, 252, 1–8. [PubMed: 17150302]

(31). Panieri E; Santoro MM ROS homeostasis and metabolism: a dangerous liason in cancer cells. Cell Death Dis. 2016, 7, e2253. [PubMed: 27277675]

(32). Hu R; Zhang X; Zhao Z; Zhu G; Chen T; Fu T; Tan W DNA nanoflowers for multiplexed cellular imaging and traceable targeted drug delivery. Angew. Chem., Int. Ed 2014, 53, 5821–5826.

(33). Mei L; Zhu GZ; Qiu L; Wu C; Chen H; Liang H; Cansiz S; Lv Y; Zhang X; Tan W Self-assembled Multifunctional DNA Nanoflowers for the Circumvention of Multidrug Resistance in Targeted Anticancer Drug Delivery. Nano Res. 2015, 8, 3447–3460. [PubMed: 27774139]

(34). Jang M; Kim JH; Nam HY; Kwon IC; JAhn H Design of a platform technology for systemic delivery of siRNA to tumours using rolling circle transcription. Nat. Commun 2015, 6, 7930. [PubMed: 26246279]

(35). Arami H; Khandhar A; Liggitt D; Krishnan KM In vivo delivery, pharmacokinetics, biodistribution and toxicity of iron oxide nanoparticles. Chem. Soc. Rev 2015, 44, 8576–8607. [PubMed: 26390044]

(36). Kievit FM; Zhang M Surface engineering of iron oxide nanoparticles for targeted cancer therapy. Acc. Chem. Res 2011, 44, 853–862. [PubMed: 21528865]

(37). Perrault SD; Walkey C; Jennings T; Fischer HC; Chan WC Mediating tumor targeting efficiency of nanoparticles through design. Nano Lett. 2009, 9, 1909–1915. [PubMed: 19344179]

(38). Szatrowski TP; Nathan CF Production of large amounts of hydrogen peroxide by human tumor cells. Cancer Res. 1991, 51, 794–798. [PubMed: 1846317]

(39). Liu C; Chen W; Qing Z; Zheng J; Xiao Y; Yang S; Wang L; Li Y; Yang R In Vivo Lighted Fluorescence via Fenton Reaction: Approach for Imaging of Hydrogen Peroxide in Living Systems. Anal. Chem 2016, 88, 3998–4003. [PubMed: 26948406]

(40). Tyagi SR; Tamura M; Burnham DN; Lambeth JD Phorbol myristate acetate (PMA) augments chemoattractant-induced diglyceride generation in human neutrophils but inhibits

phosphoinositide hydrolysis. Implications for the mechanism of PMA priming of the respiratory burst. J. Biol. Chem 1988, 263, 13191–13198. [PubMed: 2843513]

(41). Ishikawa K; Takenaga K; Akimoto M; Koshikawa N; Yamaguchi A; Imanishi H; Nakada K; Honma Y; Hayashi J ROS-generating mitochondrial DNA mutations can regulate tumor cell metastasis. Science 2008, 320, 661–664. [PubMed: 18388260]

(42). Wang R; Zhu G; Mei L; Xie Y; Ma H; Ye M; Qing FL; Tan W Automated Modular Synthesis of Aptamer–Drug Conjugates for Targeted Drug Delivery. J. Am. Chem. Soc 2014, 136, 2731–2734. [PubMed: 24483627]

(43). Wen J; Tao W; Hao S; Iyer SP; Zu Y A unique aptamer-drug conjugate for targeted therapy of multiple myeloma. Leukemia 2016, 30, 987–991. [PubMed: 26242462]

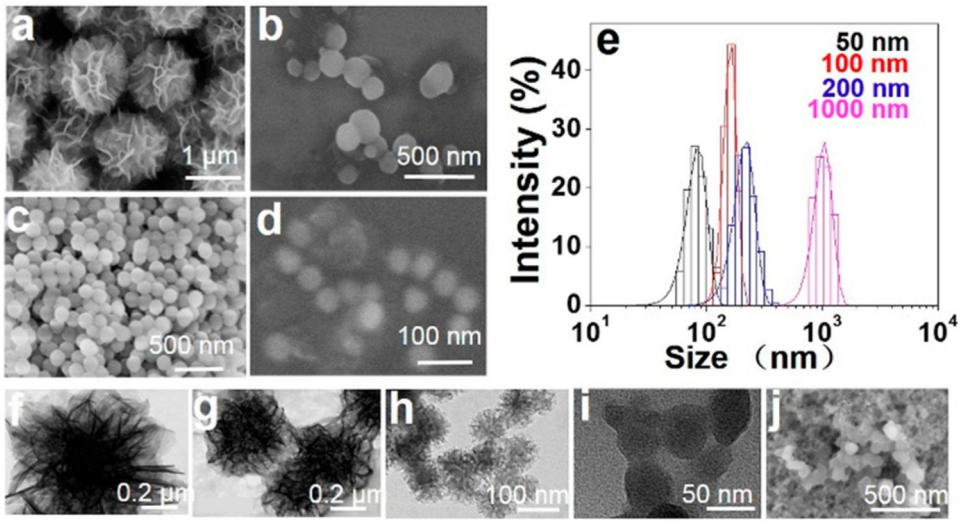

Figure 1.

SEM images of Sgc8-NFs-Fc with different sizes. (a) 1000 nm Sgc8-NFs, (b) 200 nm Sgc8-NFs-Fc, (c) 100 nm Sgc8-NFs-Fc, and (d) 50 nm Sgc8-NFs-Fc. TEM images of Sgc8-NFs-Fc with different sizes. (f) 1000 nm Sgc8-NFs, (g) 200 nm Sgc8-NFs-Fc, (h) 100 nm Sgc8-NFs-Fc, and (i) 50 nm Sgc8-NFs-Fc. (e) Hydrodynamic sizes of Sgc8-NFs-Fc with different sizes. (j) SEM images of Sgc8- NFs-Fc treated with H_2O_2.

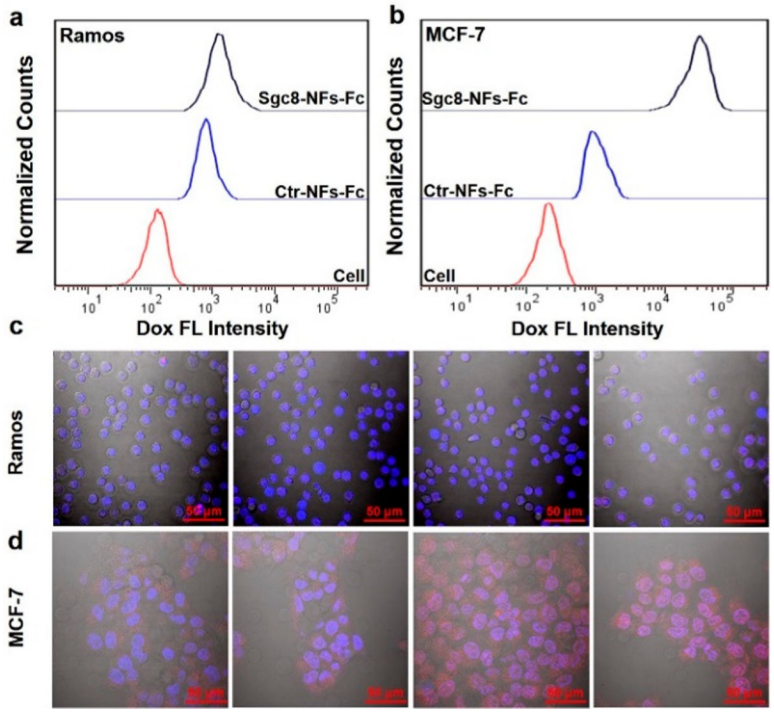

Figure 2.

Flow cytometry analysis and CLSM analysis of the targeting ability of Sgc8-NFs-Fc/Dox in PTK7- Ramos cells (a and c) and PTK7+ MCF-7 cells (b and d).

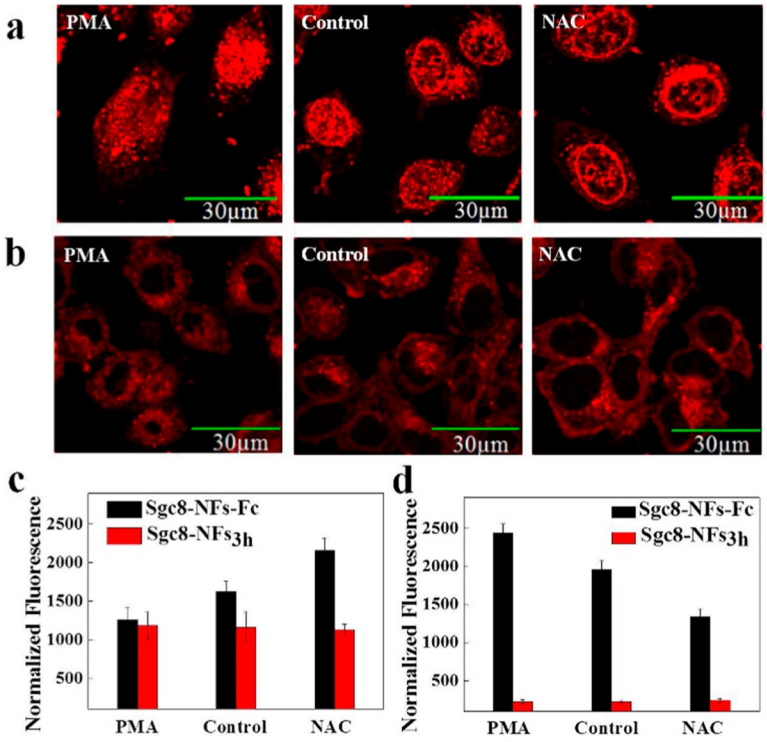

Figure 3.

Distribution of Dox in MCF-7 cells pretreated with H_2O_2 stimulant PMA or H_2O_2 scavenger NAC compared to that of native MCF-7 cells after incubation with (a) Sgc8-NFs-Fc/Dox and (b) Sgc8-NFs_{3h}/Dox. The pretreatment time of PMA or NAC was 1 h. (c) The bars represented the relative fluorescence intensity in the cytoplasm of cancer cells in a and b. (d) The bars represent the relative fluorescence intensity in nuclei of cancer cells in a and b. Bars represent the mean ± SD (n = 3).

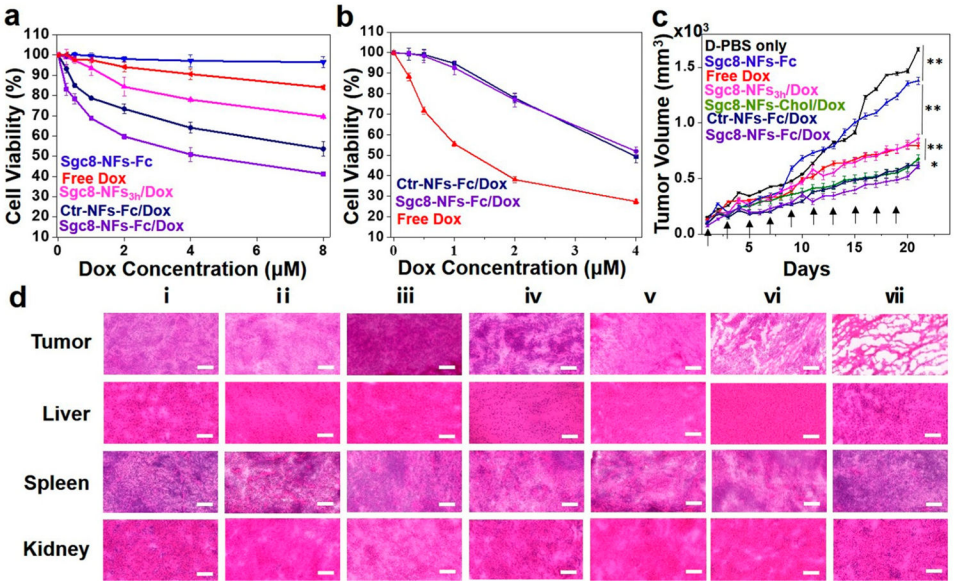

Figure 4.

In vitro cytotoxicity of Sgc8-NFs-Fc/Dox and other Dox formulations in MCF-7 cells (a) and Ramos cells (b). In vivo therapeutic efficacy analysis of Sgc8-NFs-Fc/Dox and other Dox formulations on mice bearing HCT-116 tumors: (c) tumor growth curves of different mouse groups during the 21-day treatment. Each point represents the mean ± SD. Mice were euthanized when the tumors reached ~1600 mm^3 (n = 4 for each group). Black arrows in panel c mark treatment. (d) Representative H&E staining of tumors and normal organs collected from different groups of mice 21 days post-treatment. (i) D-PBS only, (ii) free Dox, (iii) Sgc8-NFs-Fc, (iv) Sgc8-NFs-Chol/Dox, (v) Sgc8-NFs_{3h}/Dox, (vi) Ctr-NFs-Fc/Dox, and (vii) Sgc8-NFs-Fc/Dox. Each point represents the mean ± SD. Mice were euthanized when tumors reached ~1600 mm^3 (n = 4 for each group). The scale bar represents 100 μm.

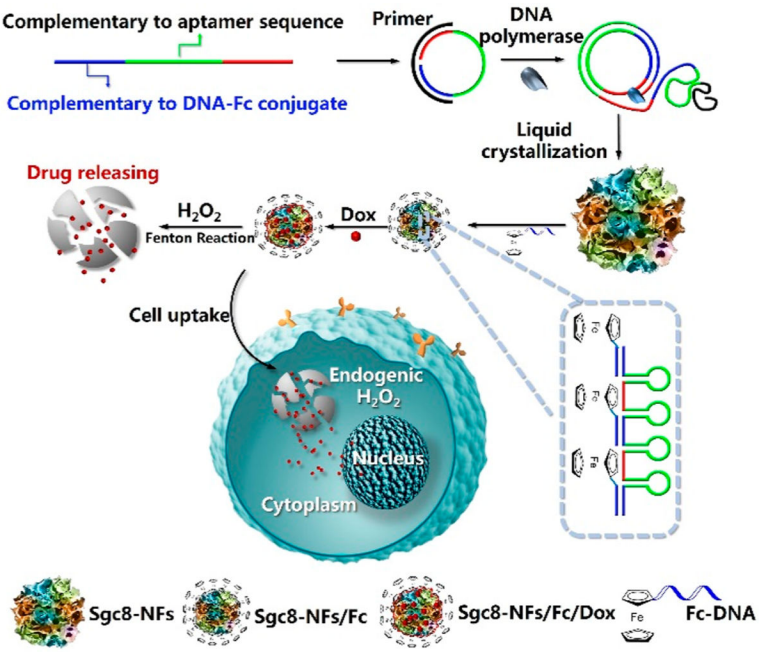

Scheme 1.

Cartoon Illustration of the Preparation of the Sgc8-NFs-Fc Nanocarrier and Its Self-Degradation via Fenton's Reaction in Cancer Cells

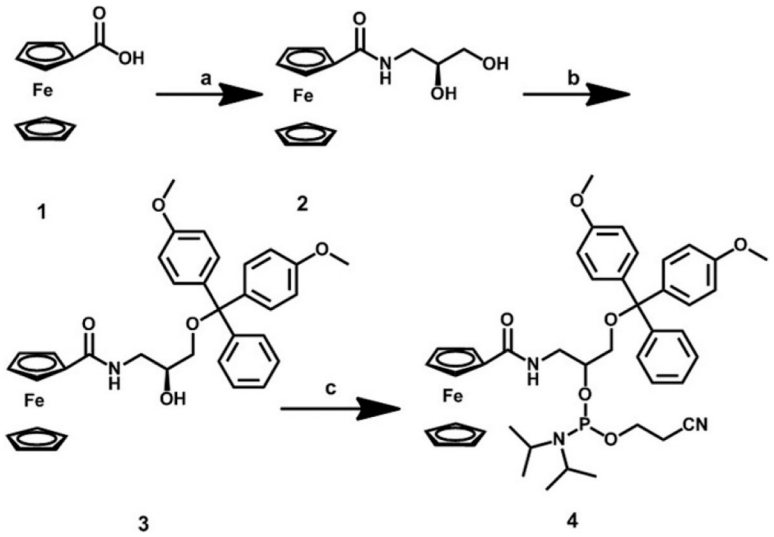

Scheme 2.

(a) (S)-3-Amino-1,2-propanediol, HBTU, DIPEA, and DMF, (b) 4,4′-Dimethoxytrityl Chloride and Pyridine, and (c) Chlorophosphoramidite and DCM